Asymmetrically Coupled Plasmonic Core and Nanotriplet Satellites

ARTICLE *in* THE JOURNAL OF PHYSICAL CHEMISTRY C · AUGUST 2014

Impact Factor: 4.77 · DOI: 10.1021/jp505024k

THE JOURNAL OF PHYSICAL CHEMISTRY C

Article

pubs.acs.org/JPCC

Asymmetrically Coupled Plasmonic Core and Nanotriplet Satellites

Hanggochnuri Jo,[†] Daesung Yoon,[‡] Ahrum Sohn,[§] Dong-Wook Kim,[§] Yeonho Choi,[∥] Taewook Kang,[∥] Dukhyun Choi,*[,‡] Sang-Woo Kim,*[,†] and Luke P. Lee*[,∥]

[†]School of Advanced Materials Science and Engineering, SKKU Advanced Institute of Nanotechnology (SAINT), Center for Human Interface Nanotechnology (HINT), Sungkyunkwan University, Suwon 440−746, Republic of Korea

[‡]Department of Mechanical Engineering, College of Engineering, Kyung Hee University, Yongin 446-701, Republic of Korea

[§]Department of Physics, Ewha Womans University, Seoul 120-750, Republic of Korea

[∥]Biomolecular Nanotechnology Center, Berkeley Sensor and Actuator Center, Department of Bioengineering, University of California at Berkeley, Berkeley, California 94720, United States

Supporting Information

ABSTRACT: Here, we report asymmetrical multiple electromagnetic coupling of plasmonic core and nanotriplet satellites. Within the plasmonic core and nanotriplet satellites, an enhanced local field is generated which expands across the core due to multiple electromagnetic coupling between a core and nanotriplets. Based on 3D simulations of our plasmonic nanosystem, the overall local field enhancement reaches to over 10^4 times, compared with that of a single nanoparticle array. A strong local field distribution across the core to nanotriplets as well as the critical role of the plasmonic core is demonstrated through the 3D simulations. It is proposed that a self-assembled nanotriplet array is completed through two stages of dewetting of a gold thin film on an anodic aluminum oxide (AAO) template. Formation of the core−nanotriplet satellites is significantly influenced by geometrical parameters (i.e., the pore diameter and depth) of the AAO template. Our experimental results show that the local field of our plasmonic nanostructures is amplified up to ∼110 times by adopting a core into the nanotriplet satellites, compared with that of the nanotriplets array without a core. This approach offers a promising strategy for creating an advanced nanoplasmonic platform with strong local field distribution and high-throughput production.

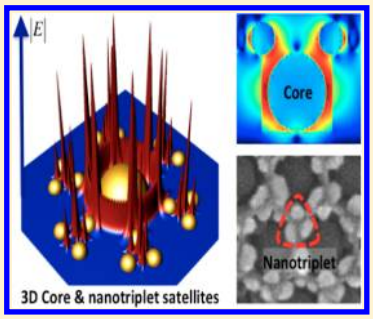

1. INTRODUCTION

The strong electromagnetic field deriving from the localized surface plasmon resonance (LSPR) on plasmonic nanostructures is key to creating high-performance optical energy devices[1−5] and highly sensitive molecular sensors.[6−10] Many studies[11−17] have thus aimed to create plasmonic nanostructures with ultrahigh electromagnetic field enhancement which is achieved near the gap between closely spaced metal nanoparticles (NPs) due to electromagnetic coupling between the localized surface plasmon (LSP) modes, constituting a "hot spot". Recently, the plasmonic coupling in multi-nanoparticle assemblies has gained increasing research interest.[18−23] Once the plasmon modes of the individual NPs are coupled together, spatial distribution of the electromagnetic field is modified and its optical spectral response is varied. In most of such coupled metallic nanostructures, the metallic NPs were symmetrically located in the same geometric plane (i.e., two-dimensional (2D) arrangement) and an enhanced field appeared only in a restricted region. It is therefore highly desirable to understand and design the electromagnetic field coupling of three-dimensional (3D) plasmonic multinanoparticle systems, where hybridization of individual LSP modes might give rise to new types of plasmon modes.

Recently, some groups have introduced 3D symmetric plasmonic clusters by using DNA strands and silanes and interestingly reported their synthesis and tunable optical characteristics.[24−26] Our group has also reported a 3D plasmonic structure by using anodic aluminum oxide (AAO) templates and dewetting process, but it was not symmetrical structure in the thickness direction.[27] We created a plasmonic single NP hexagonal array (named by nanocrown) on the AAO pore and a large core NP in the AAO pore, thus leading an asymmetrical structure in the AAO thickness direction. However, we only focused on the formation of a single NPs array on AAO which only provides a limited coupling between single NPs in a 2D domain. Their optical coupling in the asymmetrical structure is critically important to create enhanced plasmonic local field and to modify their electromagnetic field distributions, but we did not have a solution for a multiple coupled 3D plasmonic system. In this study, we thus report asymmetrical multiple coupling effects between a plasmonic core and a nanotriplet array. Effective electromagnetic coupling could be realized by self-assembling hexagonally arrayed nanotriplets on an AAO template, which are created by a controlled dewetting process of a gold thin film evaporated on an AAO template. We clearly propose and demonstrate their formation mechanism. An electric field enhancement and distribution in the core and nanotriplet

Received: May 22, 2014
Revised: July 21, 2014
Published: July 25, 2014

   dx.doi.org/10.1021/jp505024k | J. Phys. Chem. C 2014, 118, 18659−18667

structure are simulated and analyzed by 3D computational electrodynamics calculations based on the finite-difference time-domain (FDTD) method. The structural transformation by dewetting of the gold thin film on AAO is analyzed systematically according to the pore diameter and depth of AAO as well as the gold thickness. We investigate the optical behavior of the core and nanotriplet array before and after dewetting and its relation to geometrical parameters (the pore diameter and depth) of the AAO. The observed strong electromagnetic enhancement is further examined via the surface-enhanced Raman scattering (SERS) spectra of rhodamine 6G (R6G).

2. EXPERIMENTAL DETAILS

2.1. 3D Optical Simulation. We performed the FDTD simulation (Lumerical FDTD Solutions) to understand the plasmonic interactions and field distributions in the core and nanotriplet array. At first, arrays of gold NPs and nanotriplets (diameter of 25 nm) on an AAO template were modeled (no core was included in both of the cases). The array had hexagonal symmetry due to the honeycomb structure of AAO. A properly chosen unit cell was embedded in air with perfectly matched layers on the top and bottom, and with periodic boundary conditions at the sidewalls. The incident light is directed normal to the sample surface and polarized perpendicular to the propagation direction in this simulation. We applied the wavelength of 633 nm for electric field distribution of our models. For the optical simulation of the core and nanotriplet array, the gold cores (diameter of 60 nm) and the nanotriplets (diameter of 25 nm) resting on an AAO template were modeled. Spatial maps of the normalized field intensity (i.e., field enhancement) were presented to explicitly demonstrate the plasmonic field localization effect. The optical reflectance spectra were obtained by measuring the amount of power flowing into and out of the sample surfaces. We also checked the polarization effects on our model.

2.2. Preparation of AAO Template. AAO templates with hexagonally arrayed nanopores are typically fabricated by two-step anodization of aluminum. A pure aluminum (Al) sheet (99.999%) of thickness 0.5 mm was electropolished in a mixture of perchloric acid and ethanol ($HClO_4$:C_2H_5OH = 1:4 volumetric ratio) to remove surface irregularities, at a constant voltage of 20 V and at temperature 7 °C. Next, 0.3 M oxalic acid solution was used to fabricate AAO structures having an initial pore diameter 30 nm without a widening process and a periodic pore-to-pore distance (λ) of 100 nm for 12 h (first anodization) at 40 V and 15 °C. After that, the AAO layer was removed in a mixture of 1.8 wt % chromic acid and 6 wt % phosphoric acid for 6 h at 65 °C. The highly ordered AAO templates were obtained by a second anodization under the same conditions as the first anodization. The AAO depth is determined by the duration of the second anodization. To increase the AAO pore size, the AAO templates were etched in 0.1 M phosphoric acid at 30 °C.

2.3. Intermediately Dewetted Sample Preparation. To prepare the dewetted gold nanoparticles on an AAO template at the intermediate temperature, the gold-coated AAO substrate was carefully immersed in nitrogen for quenching as soon as the annealing temperature reached at 400 °C.

3. RESULTS AND DISCUSSION

3.1. Electromagnetic Coupling Model for a Plasmonic Core−Nanotriplet System. We propose a 3D plasmonic multi-nanoparticle system, consisting of a metallic core at the center and nanotriplet satellites, as shown in Figure 1a(ii). The

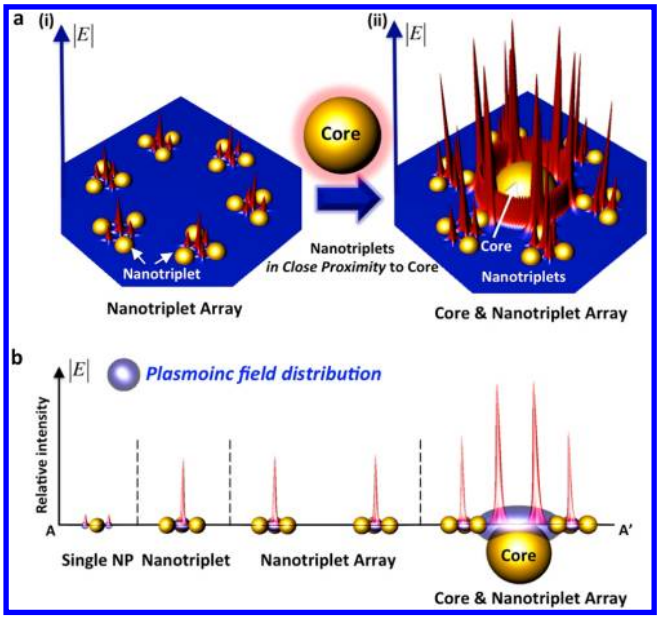

Figure 1. Multiple coupling of electromagnetic fields in asymmetrical plasmonic core and hexagonally arrayed nanotriplet satellites. (a) Scheme for ultrahigh local field generation through multiple electromagnetic coupling in a core and hexagonally arrayed nanotriplet structure. (b) Illustration of local field intensity (E) and distribution (blue area) in single NP, nanotriplet, hexagonally arrayed nanotriplet, and asymmetrical core and hexagonally arrayed nanotriplet structures.

system has a hexagonally arrayed nanotriplets (Figure 1a(i)), in which collective resonance among the NPs generates a strong local field in the gap (<10 nm) between the neighboring NPs. With a large core at the center of the nanotriplet array, further asymmetrical plasmonic coupling enables hybridization of the localized modes in the core and the nanotriplets, thus forming enhanced local field distribution in a large volumetric space (see the schematic illustration in Figure 1a(ii)) between the core and the nanotriplet satellites.

Figure 1b illustrates the electric field distribution in the core and nanotriplet satellites upon adopting a core into hexagonally arrayed triplets. A plasmonic single NP provides an enhanced local field in the vicinity of the NP (see Figure 1b). When a nanotriplet is formed with a gap less than 10 nm, the NPs can be regarded as point dipoles interacting via their near-field and strong field localization in the nanosized gaps between adjacent particles appears.[28] Furthermore, the hot spot (the blue region in Figure 1b) of the nanotriplet will occupy larger spatial volume near the constituent NPs compared with that of a single isolated NP. If a hexagonal array of the nanotriplets is formed, further enhanced local field is expected due to the coupling between nanotriplets and also the spatial volume of hot spots will increase. Asymmetrical addition of a metal core to the nanotriplet array completes a 3D multinanoparticle plasmonic system, where hybridized plasmon mode can be formed. Such multiple plasmon coupling will lead to much larger spatial volume of hot spots and alteration of spectral optical response. The 3D asymmetrical multinanoparticle plasmon system with

dx.doi.org/10.1021/jp505024k | J. Phys. Chem. C 2014, 118, 18659−18667

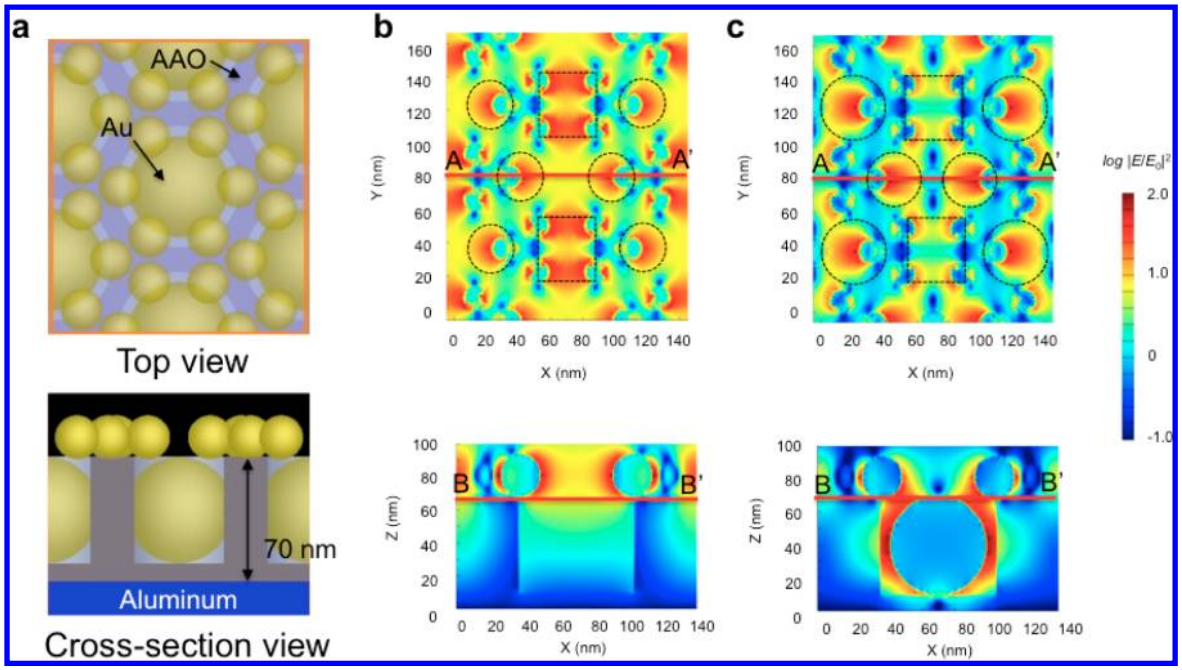

Figure 2. 3D optical simulation for local field enhancement and distribution. (a) Top and cross-sectional views of schematic diagrams for the core–nanotriplet array used in the simulation. Normalized electric field intensity ($|E/E_0|^2$) distributions of (b) the nanotriplet array only (without the cores) and (c) the asymmetrical core–nanotriplet array at incident light wavelength ($\lambda_{incident}$) of 633 nm (E_0: the electric field of incident light). The electric field at the top view is the plane of B–B′ in the cross section, and its cross-sectional field distribution is the plane of A–A′ in the top view.

an enhanced local field and its large spatial distribution (i.e., spacious volume of hot spots) can thus be a new type of platform to realize high-performance optical energy devices, such as solar cells and LEDs integrated with nanoplasmonic structures, as well as nanoplasmonic molecular analytic devices for bio/medical/environmental applications.

3.2. 3D Optical Simulations. To describe the electromagnetic field distribution in the core and nanotriplet satellites, we solved the Maxwell equations by the FDTD method (see Experimental Details and Figure S1 for the details). The periodic array was modeled in FDTD (Lumerical FDTD Solutions) as shown in Figure 2a. We first compared the electric fields from a single NP array on AAO and a nanotriplet array on AAO (see Figure S2). The maximum normalized electric field from a nanotriplet array on AAO was about 4 times greater than that from a single NP array on AAO, which corresponds to the enhancement factor (EF) of ~250.[29] Furthermore, the enhanced electric fields from the nanotriplet array on AAO were distributed in the significantly wide region (i.e., increased spatial volume of hot spots; roughly reaches to over 2 times). Thus, it can be clearly understood that the nanotriplet array is greatly effective for electric field enhancement.

In order to understand the role of the core in the 3D multinanoparticle system, we compared the calculated electric field distributions of the nanotriplet array only on AAO (i.e., without a core) and the core–nanotriplet satellites on AAO, as shown in Figures 2b,c (also see Figure S3). Plasmonic coupling in the closely spaced nanotriplets was clearly observed (see the dot squares in Figure 2b), but low electric fields inside the AAO pore were distributed (see cross-sectional field distribution in Figure 2b). By adopting the plasmonic core in the nanotriplet array on AAO (i.e., inside the AAO pore), the electric field distribution around the core and the nanotriplets are greatly modified due to the asymmetrical multiple electromagnetic coupling among the NPs (see Figure 2c and Figure S3). It should be noted that the near-field intensity near the plasmonic core is strongly confined in the AAO pore. Since the AAO has a large dielectric constant, the field cannot easily penetrate into the AAO. The hot-spots of the core-nanotriplet array can be found at the core vicinity and the core-nanotriplet gaps. This indicates that the plasmonic coupling between the localized modes of the core and the nanotriplet occurs, significantly influencing the optical properties of the 3D plasmonic nanostructure. Such a strong coupling effect between the core and the nanotriplets could be found in the reflectance spectra (see Figure S4a). The scattering resonance of the core–nanotriplet system is critically dependent to the core only system, not to the nanotriplet only system. Furthermore, the core–nanotriplet system did not depend on the polarization direction (see Figure S4b). Interestingly, strong local fields in somewhere of the nanotriplet array were quite suppressed in the core–nanotriplet array (see the dot squares in Figure 2b,c), since the dipole fields from the core and the nanotriplets have opposite directions at the positions. This behavior shows good agreement with that of heptamer in the previous study.[18] On the other hand, the enhanced fields around the core of the 3D plasmonic system were obviously distributed in a significantly extended volume (see the dot circles on the top view and the cross section in Figure 2c) compared with that of the simple 2D array systems (i.e., a nanotriplet array only). The spatial volume of enhanced local fields in the 3D core–satellites system was roughly 5 times larger than that of 2D nanotriplet arrays, which means the EF of ~25 (see Supporting Information). By considering the enhanced intensity of electric fields and their increased spatial volume, the overall EF of our 3D core–satellites system thus reaches to approximately over 10^4, compared with that of a 2D single NP array system (see Figure S2a).

dx.doi.org/10.1021/jp505024k | J. Phys. Chem. C 2014, 118, 18659–18667

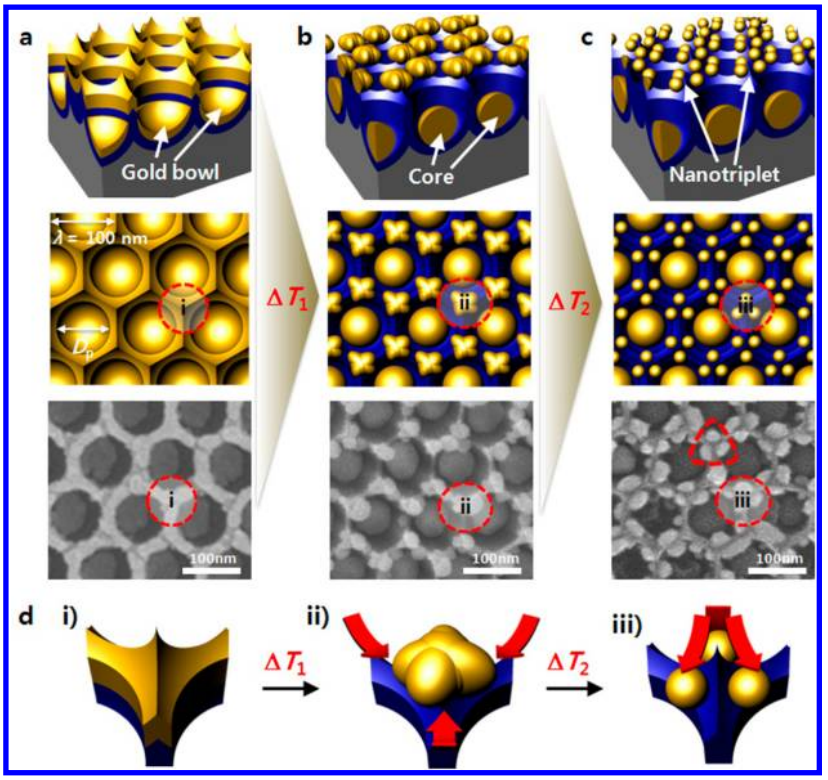

Figure 3. Mechanism for nanotriplet formation on AAO via dewetting. (a) Evaporated gold on AAO template. The gold thickness was 20 nm. Separated gold bowls were formed in each AAO nanopore. (b) Intermediately dewetted gold on AAO at 400 °C (ΔT_1). (c) Plasmonic nanotriplet array formed by dewetting at 600 °C (ΔT_2) for 3 h. (d) Proposed mechanism for the formation of gold nanotriplet on AAO by dewetting.

In 2D plasmonic nanostructures, major factors to determine the optical properties include the materials (metals and dielectric media), the size and shape of the NPs, the nanogap spacing, and the symmetry of the NP array. In 3D systems, the separation between neighboring NP-containing planes and the 3D arrangement (particularly, asymmetrical arrangement) of the NPs provide us additional degrees of freedom to tailor their optical characteristics.[19] In spite of such fascinating features of the 3D system, fabrication of the 3D nanostructures usually require quite time-consuming, labor-intensive, and expensive fabrication processes. This hampers investigations of various 3D plasmonic systems and understanding their intriguing plasmonic coupling behaviors.

3.3. Fabrication and Proposed Mechanism for a Large-Area Nanotriplet Array. The plasmonic core and nanotriplet array shown in Figure 1a(ii) was created by dewetting a gold thin film on an AAO template having hexagonally ordered nanopores which was prepared by two-step anodization (details in the Experimental Details).[30,31] The periodic distance (λ) between nanopores in AAO was 100 nm, and the AAO pore diameter (D_p) was about 80 nm. A gold thin film, of thickness 20 nm, was evaporated onto the AAO (Figure 3a). Annealing for 3 h at 600 °C (ΔT_2) then created a self-assembled core and nanotriplet array on AAO (Figure 3c). A gold nanotriplet (see the triangular area of the field emission scanning electron microscopy (FE-SEM) image in Figure 3c) is formed around the vertex that interconnects three AAO nanopores (see Figure S5), and a single core is produced in an AAO nanopore. We could prepare a large-area AAO template with the size of about 3 cm^2, and the diameter of nanotriplet was distributed between 15 and 30 nm (about 22 nm in average) as shown in Figure S6. Our nanofabrication processes are not top-down nanolithography, but high-throughput bottom-up self-assembly. Consequently, our nanofabrication method has the benefits of high throughput, large-area uniformity, reproducibility, and cost-effectiveness.

To clearly understand the mechanism of the nanotriplet formation on AAO by dewetting, we monitored the samples annealed at an intermediate temperature of 400 °C (ΔT_1) (see details of the sample preparation in the Experimental Details) and observed FE-SEM images before (Figure 3a(i)) and after (Figure 3c(iii)) dewetting as well as at the intermediate temperature (Figure 3b(ii)). On the basis of the FE-SEM images (particularly the dotted areas (i)−(iii)), we suggest that dewetting proceeds in two stages in the nanotriplet formation on AAO. As the temperature increases, the thin gold film on AAO (Figure 3d(i)) first aggregates on the vertex (Figure 3d(ii)) connecting three AAO nanopores due to atomic diffusion[32] and the local excess chemical potential.[33] As shown in Figure S5a, the AAO template has a sharp vertex connecting three nanopores and six curved perimeters around the entrance of a nanopore. As a result of the geometrical characteristics of the AAO template, a thicker gold layer is formed by evaporation on the vertex and a relatively thin layer on the curved perimeters (see Figure S5c).[34] In general, atomic diffusion progresses from smaller particles to the largest. Thus, gold atoms diffuse away from the thin layer on the perimeters to the thicker layer on the vertex, finally forming an aggregated gold particle at the vertex (see Figure 3d(ii)). Furthermore, the Gibbs−Thomson relation[33] allows the gold atoms to diffuse away from the perimeter to the vertex. (This relation is $\Delta\mu = \kappa\gamma\Omega$, where $\Delta\mu$ is the local excess chemical potential, κ is the local curvature, γ is the surface energy, and Ω is the atomic volume.) This is because the local excess chemical potential is

dx.doi.org/10.1021/jp505024k | J. Phys. Chem. C 2014, 118, 18659−18667

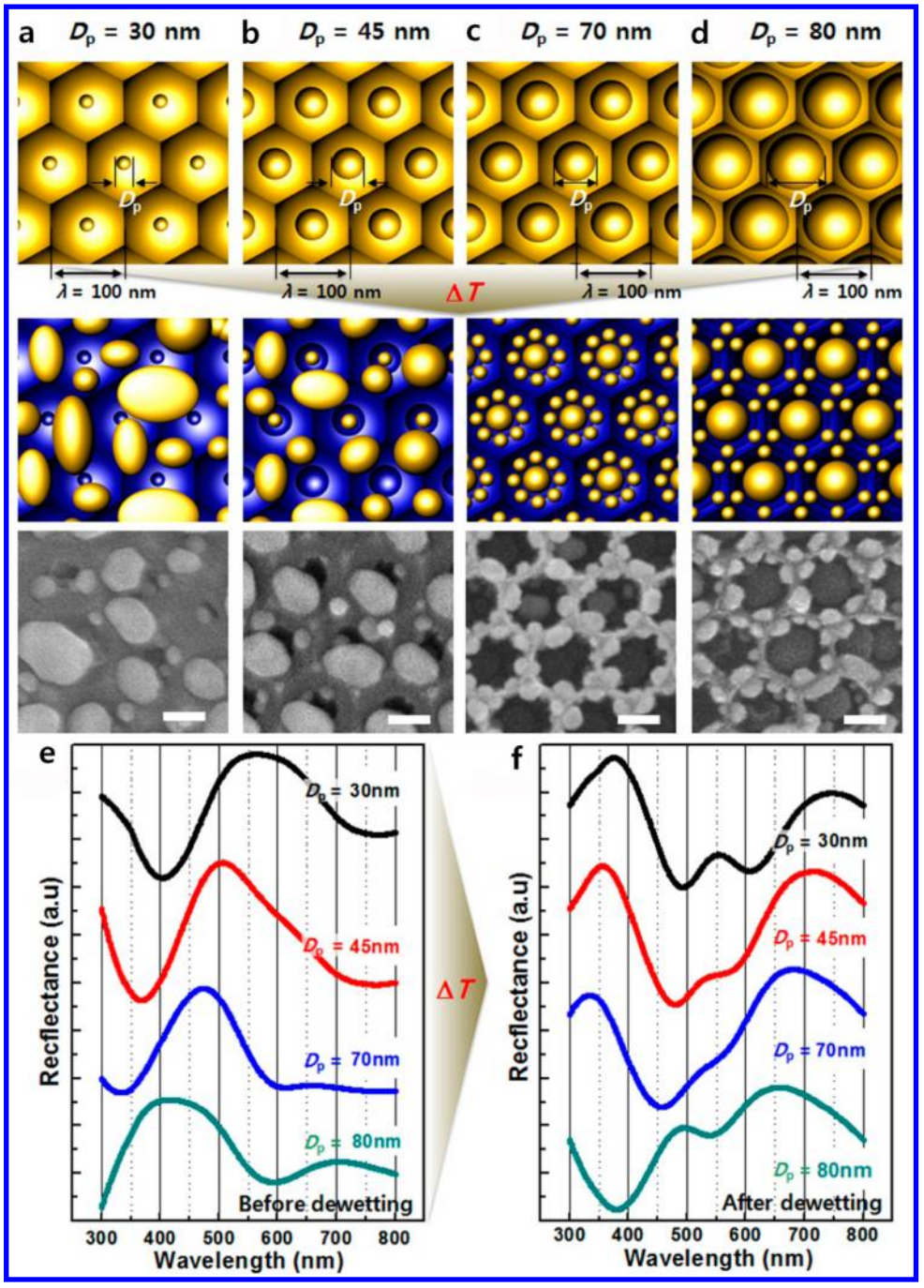

Figure 4. Dewetting behaviors of gold on AAO according to the AAO pore size. Schematics and FE-SEM images for dewetted gold on AAO with different pore size (D_p) (a) 30, (b) 45, (c) 70, and (d) 80 nm. Corresponding optical reflectance spectra (e) before and (f) after dewetting.

reduced by the gold aggregating on the vertex. For the AAO nanopore, there is a negative local excess chemical potential at the perimeter that is proportional to the local curvature ($\kappa_p = -1/|R_p|$), and a positive excess chemical potential at the vertex that is proportional to the local curvature ($\kappa_v = 1/R_v$) (see Figure S5c). As the annealing process progresses, the evaporated gold atoms diffuse from the perimeter toward the vertex so as to reduce the local excess chemical potential by increasing the radius of curvature (R_v) at the vertex.

When the annealing temperature reaches 600 °C (ΔT_2) and is maintained for 3 h, the gold particle aggregated on the vertex becomes more viscous (i.e., like a liquid metal) and flows down from the top of the vertex into the inside wall of the vertex (Figure 3d(iii)), where it finally divides into three small particles, forming a nanotriplet. Obviously, this division of an aggregated gold particle into a nanotriplet minimizes the surface energy, but the geometrical parameters of the AAO template have a significant influence on the formation of the nanotriplets.

To investigate the effect of the AAO pore size on the formation of nanotriplets, we prepared AAO templates having different pore diameters (D_p) of 30, 45, 70, and 80 nm (see the FE-SEM images in Figure S7). The periodicity (λ) of the AAO pores was 100 nm. 20 nm thick gold was evaporated on AAO, and the films were annealed at 600 °C (ΔT) for 3 h. As shown in Figure 4, the randomly dewetted NPs on the AAO template

dx.doi.org/10.1021/jp505024k | J. Phys. Chem. C 2014, 118, 18659−18667

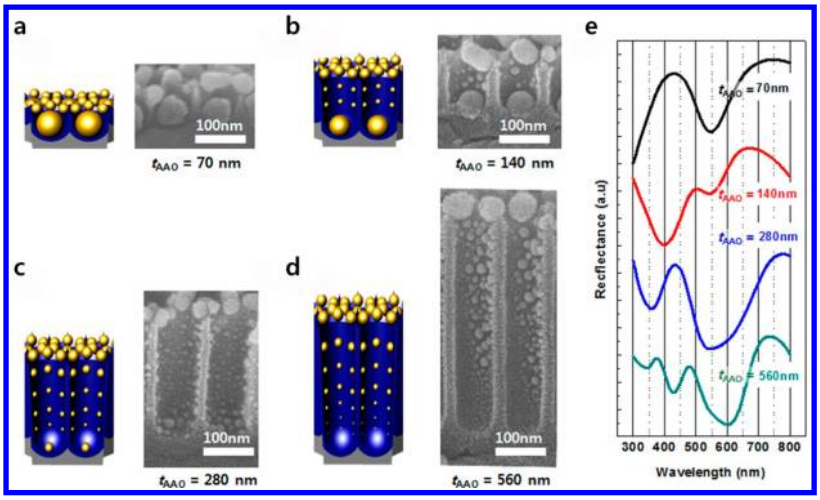

Figure 5. Effect of AAO depth on the core formation. Cross-sectional schematics and FE-SEM images for dewetted gold on AAO with different depth (t_{AAO}) (a) 70, (b) 140, (c) 280, and (d) 560 nm. The AAO pore diameter was 80 nm, and the gold thickness was 20 nm. (e) Corresponding optical reflectance spectra.

with D_p = 30 nm were formed and did not interact with the template. We believe that this is due to the large surface area around the AAO pores, on which the driving force for flow toward the vertex is smaller due to the similar thick gold layer on the surface (i.e., weak atomic diffusion toward the vertex) and also the large radius of curvature at the surface around the AAO pores (i.e., low local excess chemical potential). As the AAO pore size increases, the dewetted nanoparticles are observed to collect around the entrance to the AAO pore (see Figure 4c), finally well forming nanotriplets on the AAO template with D_p = 80 nm (see Figure 4d). The size of the dewetted gold nanoparticles in the nanotriplet was measured to be ~22 nm on average and the gap in the nanotriplet was ~10 nm, which is an excellent value for enhancing the electromagnetic field

We also examined the corresponding optical behavior before and after dewetting of the gold thin film on the AAO templates, as shown in Figure 4e,f. Before annealing, gold evaporated on the AAO showed a single LSPR dip in the visible range, which was progressively blue-shifted as the AAO pore size increases. This is due to the decrease of the effective dielectric constant of the dielectric medium surrounding the metal nanostructures, as the AAO pore size increases. A high permittivity substrate can reduce the LSPR energy due to strong image charge with larger interactions with the oscillating electrons.[35] The effective dielectric constant of the AAO beneath the gold layer can be estimated from the Maxwell−Garnett equation,[36] in which the volume fraction of air and alumina is taken into account. Based on the SP dispersion relation, the LSPR of the gold evaporated on AAO should be blue-shifted as D_p increases, since the effective dielectric constant of the AAO template decreases as D_p increases. After dewetting of the gold layer on AAO, multiple LSPR dips were observed, due presumably to the multiple particle sizes as well as the multiple electromagnetic coupling effects in nanotriplets. Isolated symmetric trimer belongs to the D_{3h} point group, and collective plasmon modes of the trimer can be constructed from linear combination of individual NP plasmon modes.[37,38] When the nanotriplet composes a hexagonal array on AAO, plasmon hybridization modes are quite different from those of the isolated trimer.[39] By adopting the core into the nanotriplet array, the strong field around the core weakens the coupling between the nanotriplets (see Figure 2c) and plasmonic coupling between NPs in the nanotriplet is similar to that of the isolated trimer. Thus, the reflectance spectra of Figure 4f can be partly explained by the multiple plasmon resonances, but it should be further investigated since our system is complicatedly related with trimer characteristics,[37,38] Fano resonance,[18] and interference.[40]

Since the dewetting behavior is critically sensitive to the local curvature of the template, as well as the continuity of evaporated thin films, the thickness (t_{Au}) of the evaporated gold layer is very important. If the gold layer is initially too thin, the evaporated gold may be discontinuous on the AAO and randomly dispersed holes exist in the gold layer, so that multiple dewetted nanoparticles upon annealing self-form immediately at the random sites, instead of dewetting taking place by the rupture of the thin film on the template (see Figure S8a for t_{Au} = 5 nm). As the thickness of the gold layer increases, the dewetted nanoparticles form around the AAO pores and the geometry-dominant dewetting (i.e., rupture of the gold thin film interacting with the AAO template) progresses (see Figure S8b,c for t_{Au} = 10 and 20 nm). However, too thick a gold layer reduces the local curvatures and produces continuous film between the gold layer on the perimeter and the gold bowl in the AAO pore, so that randomly dispersed large nanoparticles are finally formed on the AAO (see Figure S8d for t_{Au} = 30 nm).

3.4. Formation and Role of a Plasmonic Core Nanoparticle. To achieve 3D multiple electromagnetic coupling in the plasmonic core and nanotriplet structure, the formation of the core is critically important, as demonstrated in 3D optical calculations of Figure 2. When gold is evaporated on AAO, a gold bowl (see Figure 3a) is formed at the bottom of an AAO pore, without any linking with the gold layer at the entrance of the pore. Consequently, an independent large gold core is formed in an AAO pore during the annealing process. Core formation during dewetting gold on AAO depends critically on the AAO depth (t_{AAO}). Figure 5 shows cross-sectional FE-SEM images of dewetted gold on AAO according to the AAO depth. We fabricated the AAO templates with D_p= 80 nm and t_{AAO} = 70, 140, 280, and 560 nm, and a 20 nm thick gold was evaporated onto the AAO templates. Based on the FE-SEM images after dewetting, the corresponding core size was approximately 50 nm for t_{AAO}= 70 (Figure 5a) and 35 nm for

dx.doi.org/10.1021/jp505024k | J. Phys. Chem. C 2014, 118, 18659−18667

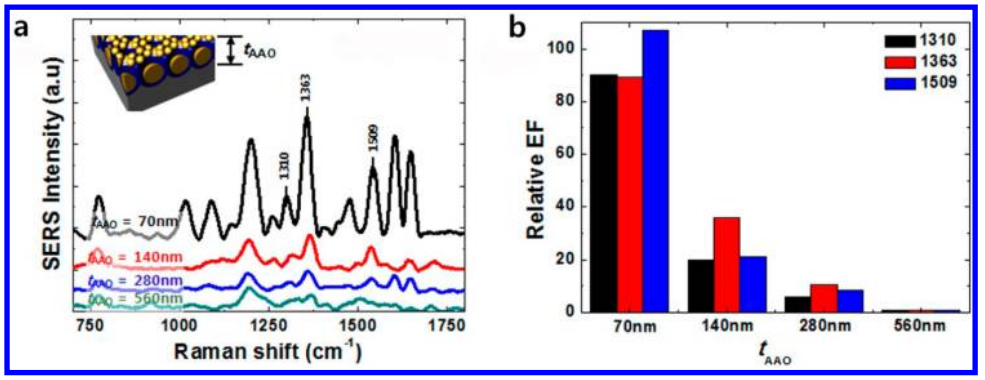

Figure 6. Quantitative electromagnetic field enhancement of the asymmetrical plasmonic core and nanotriplet array structures with different AAO depths. (a) SERS spectra of 1 μM R6G on four plasmonic nanostructures shown in Figure 5. (b) Relative enhancement factor (EF) for the plasmonic nanostructures with different AAO depths. It was determined at the three main Raman peaks (1310, 1363, and 1509 cm^{-1}) for R6G and the SERS spectra of the plasmonic nanostructure with t_{AAO} = 560 nm as the reference value.

t_{AAO}= 140 nm (Figure 5b); no cores were created for t_{AAO} = 280 and 560 nm (Figure 5c,d). Obviously, gold atoms are deposited both on the bottom and the inside wall of AAO pores during evaporation, but they could not reach the bottom of the AAO pore when the pore is deep. Consequently, no core was formed at the bottom of the AAO pores upon annealing, and only small particles were formed at the wall of the pores, as shown in Figure 5c,d. In contrast, a single large core was formed at the bottom of an AAO pore for the AAO template with shallow depth, as shown in Figure 5a,b. The gap between the core and the nanotriplets in Figure 5a appears to be below 10 nm in some places, which is important for enhancement of the electromagnetic field by multiple coupling between the core and the nanotriplets. The AAO surface is not perfectly flat, and the NPs have rather irregular shapes, so that the statistical variation of the minimal gaps between the NPs would be present. The reflectance spectra of the core−nanotriplet plasmonic structures with various AAO pore depths (t_{AAO}) were measured in Figure 5e. As shown in the SEM images in Figures 5a,d, t_{AAO} varies the core size as well as the core-to-nanotriplet distance. Thus, the spectral difference in Figure 5e should reflect the influence of the plasmonic coupling in the core−nanotriplet array. Multiple dips are also observed as like Figure 4f; the dip position is shifted, and the number of dips increases as increasing t_{AAO}.

From the SERS spectra of R6G by the Raman system with an excitation wavelength of 633 nm, we determined the electromagnetic enhancement factor (EF) of the plasmonic core and nanotriplet array according to the AAO depth (i.e., the effect of the core on the EF). Figure 6a shows SERS spectra of R6G of 1 μM on our plasmonic substrates. We measured SERS signals over 60 times (about 20 times on one sample and more than 3 samples), and the signal variation was below 10%. Higher SERS signals were obtained as the AAO depth decreases, since the large core is well formed and close to the nanotriplets, thus leading to higher multiple electromagnetic coupling. To determine the relative SERS EF according to the AAO depth, we used the SERS spectra of the plasmonic substrate with the AAO template having t_{AAO} = 560 nm as the reference value. The relative EF for different AAO depths was determined at the three main Raman peaks for R6G (i.e., 1310, 1363, and 1509 cm^{-1}),[41] as shown in Figure 6b. According to the measured results, the analytical EFs at each main peak were calculated from the equation EF = $(I_{SERS}/I_{Raman}) \times (C_{Raman}/C_{SERS})$, where I and C respectively denote intensity and concentration. As the AAO depth decreases, the relative EF increased, with an enhancement factor of about 110 times at 1509 cm^{-1} for our plasmonic nanostructures with the AAO template having t_{AAO} = 70 nm. This observation confirms that the role of the core in the core and nanotriplet plasmonic structure is crucially important in enhancing the electromagnetic field. Of course, the substrate surface area and the resultant detectable molecule numbers are different with the AAO pore size and depth. This study actually focuses on those points in our 3D nanoplasmonic structures. In other words, the intensity and the distribution volume of enhanced EM fields are varied with the AAO pore size and depth, so that the SERS EF could be different on our 3D nanoplasmonic structures. We further measured the SERS spectra of R6G at low concentrations up to 10 pM, demonstrating the potential for application to ultrasensitive SERS substrates. Based on the measured results and reference data, the analytical EFs at each main peak were determined to reach above 10^9.

4. CONCLUSION

In conclusion, we have demonstrated the multiple coupling behavior of a 3D asymmetrical multinanoparticle plasmonic system, consisting of a large core and hexagonally arrayed nanotriplet satellites, which has strong near-field enhancement and significantly increased volumetric distribution due to the asymmetrical multiple coupling of the individual plasmonic modes. Our nanotriplet array is more important and clearly different with nanocrown (i.e., single NP array) structures that were previously reported.[27] In the nanocrown structure, multiple coupling between single NPs could not be generated due to the large distance between single NPs. More importantly, the role of the core NP was not characterized in our previous study. In this study, we focused on the multiple coupling between nanotriplets as well as asymmetrical coupling between the core and nanotriplets. Furthermore, we provided systematic characterizations and mechanism for roles and formation of each element in our nanosystem. As a result, the 3D core and nanotriplet satellites provided 10^4 times EF, compared with that of a 2D single NP array. A two-step process for the dewetting mechanism leading to the formation of the nanotriplet on AAO was proposed, and the dependence was investigated of the morphology on the pore diameter and the depth of AAO templates as well as the gold thickness. Optical measurements of our nanoplasmonic array showed the multiple plasmonic resonances. By using SERS spectra, the local field

dx.doi.org/10.1021/jp505024k | J. Phys. Chem. C 2014, 118, 18659−18667

enhancement of our nanoplasmonic structures was measured up to 110 times depending on the core formation and the SERS EF exceeding 10^9 was found. Even though we here only used AAO templates, various nanotemplates could be further applied to design and to create 3D asymmetrical plasmonic systems based on our results. Furthermore, the multiple coupling of LSP modes and spatial distribution in 3D asymmetrical systems will pave the way for realizing high-performance optical energy/bio/medical/environmental devices with nanoplasmonic structures.

■ ASSOCIATED CONTENT

Supporting Information

Experimental and simulation details, geometrical morphology of AAO template, AAO templates with different pore diameters, Au thickness dependency, and size distribution of the dewetted particles in triplets formed on AAO template. This material is available free of charge via the Internet at http://pubs.acs.org.

■ AUTHOR INFORMATION

Corresponding Authors

*E-mail dchoi@khu.ac.kr (D.C.).
*E-mail kimsw1@skku.edu (S.-W.K.).
*E-mail lplee@berkeley.edu (L.P.L.).

Present Addresses

Y.C.: Department of Biomedical Engineering, Korea University, South Korea.
T.K.: Department of Chemical Engineering, Sogang University, South Korea.

Notes

The authors declare no competing financial interest.

■ ACKNOWLEDGMENTS

This work was financially supported by the Energy International Collaboration Research & Development Program of the Korea Institute of Energy Technology Evaluation and Planning (KETEP) funded by the Ministry of Knowledge Economy (MKE) (2011-8520010050) and by Basic Science Research Program through the National Research Foundation of Korea (NRF) funded by the Ministry of Education, Science and Technology (2013R1A1A2063798). S.-W.K. also acknowledges financial support by Basic Science Research Program (2009-0083540).

■ REFERENCES

(1) Atwater, H. A.; Polman, A. Plasmonics for Improved Photovoltaic Devices. *Nat. Mater.* **2010**, *9*, 205−213.
(2) Nakayama, K.; Tanabe, K.; Atwater, H. A. Plasmonic Nanoparticle Enhanced Light Absorption in GaAs Solar Cells. *Appl. Phys. Lett.* **2008**, *93*, 121904.
(3) Ferry, V. E.; Sweatlock, L. A.; Pacifici, D.; Atwater, H. A. Plasmonic Nanostructure Design for Efficient Light Coupling into Solar Cells. *Nano Lett.* **2008**, *8*, 4391−4397.
(4) Catchpole, K. R.; Polman, A. Plasmonic Solar Cells. *Opt. Express* **2008**, *16*, 21793−21800.
(5) Bouhelier, A.; Beversluis, M. R.; Novotny, L. Characterization of Nanoplasmonic Structures by Locally Excited Photoluminescence. *Appl. Phys. Lett.* **2003**, *83*, 5041−5043.
(6) Lim, D.-K.; Jeon, K.-S.; Kim, H. M.; Nam, J.-M.; Suh, Y. D. Nanogap-engineerable Raman-active Nanodumbbells for Single-Molecule Detection. *Nat. Mater.* **2010**, *9*, 60−67.
(7) Stokes, R. J.; Macaskill, A.; Lundahl, P. J.; Smith, W. E.; Faulds, K.; Granham, D. Quantitative Enhanced Raman Scattering of Labeled DNA from Gold and Silver Nanoparticles. *Small* **2007**, *3*, 1593−1601.
(8) Lu, Y.; Liu, G. L.; Kim, J.; Mejia, Y. X.; Lee, L. P. Nanophotonic Crescent Moon Structures with Sharp Edge for Ultrasensitive Biomolecular Detection by Local Electromagnetic Field Enhancement Fffect. *Nano Lett.* **2005**, *5*, 119−124.
(9) Dong, Z. C.; Zhang, X. L.; Gao, H. Y.; Luo, Y.; Zhang, C.; Chen, L. G.; Zhang, R.; Tao, X.; Zhang, Y.; Yang, J. L.; Hou, J. G. Generation of Molecular Hot Electroluminescence by Resonant Nanocavity Plasmons. *Nat. Photonics* **2009**, *4*, 50−54.
(10) Hong, G.; Wu, J. Z.; Robinson, J. T.; Wand, H.; Zhang, B.; Dai, H. Three-dimensional Imaging of Single Nanotube Molecule Endocytosis on Plasmonic Substrates. *Nat. Commun.* **2012**, *3*, 700.
(11) Shegai, T.; Chen, S.; Miljković, V. D.; Zengin, G.; Johansson, P.; Käll, M. A Bimetallic Nanoantenna for Directional Colour Routing. *Nat. Commun.* **2011**, *2*, 481.
(12) Su, K.-H.; Durant, S.; Steele, J. M.; Xiong, Y.; Sun, C.; Zhang, X. Raman Enhancement Factor of a Single Tunable Nanoplasmonic Resonator. *J. Phys. Chem. B* **2006**, *110*, 3964−3968.
(13) Haynes, C. L.; Van Duyne, R. P. Plasmon-Sampled Surface-Enhanced Raman Excitation Spectroscopy. *J. Phys. Chem. B* **2003**, *107*, 7426−7433.
(14) McFarland, A. D.; Young, M. A.; Dieringer, J. A.; Van Duyne, R. P. Wavelength-Scanned Surface-Enhanced Raman Excitation Spectroscopy. *J. Phys. Chem. B* **2005**, *109*, 11279−11285.
(15) Choi, D.; Choi, Y.; Hong, S.; Kang, T.; Lee, L. P. Self-Organized Hexagonal-Nanopore SERS Array. *Small* **2010**, *6*, 1741−1744.
(16) Li, S.; Pedano, M. L.; Chang, S. H.; Mirkin, C. A.; Schatz, G. C. Gap Structure Effects on Surface-enhanced Raman Scattering Intensities for Gold Gapped Rods. *Nano Lett.* **2010**, *10*, 1722−1727.
(17) Lim, D. K.; Jeon, K. S.; Hwang, J. H.; Kim, H.; Kwon, S.; Suh, Y. D.; Nam, J. M. Highly Uniform and Reproducible Surface-enhanced Raman Scattering from DNA-tailorable Nanoparticles with 1-nm Interior Gap. *Nat. Nanotechnol.* **2011**, *6*, 452−460.
(18) Hentschel, M.; Saliba, M.; Vogelgesang, R.; Giessen, H.; Alivisatos, A. P.; Liu, N. Transition from Isolated to Collective Modes in Plasmonic Oligomers. *Nano Lett.* **2010**, *10*, 2721−2726.
(19) Liu, N.; Hentschel, M.; Weiss, T.; Alivisatos, A. P.; Giessen, H. Three-Dimensional Plasmon Rulers. *Science* **2011**, *332*, 1407−1410.
(20) Halas, N. J.; Lal, S.; Chang, W.-S.; Link, S.; Nordlander, P. Plasmons in Strongly Coupled Metallic Nanostructures. *Chem. Rev.* **2011**, *111*, 3913−2961.
(21) Aćimović, S. S.; Kreuzer, M. P.; González, M. U.; Quidant, R. Plasmon Near-Field Coupling in Metal Dimers as a Step toward Single-Molecule Sensing. *ACS Nano* **2009**, *3*, 1231−1237.
(22) Fan, J. A.; Wu, C.; Bao, K.; Bao, J.; Bardhan, R.; Halas, N. J.; Manoharan, V. N.; Nordlander, P.; Shvets, G.; Capasso, F. Self-Assembled Plasmonic Nanoparticle Clusters. *Science* **2010**, *328*, 1135−1138.
(23) Ye, J.; Wen, F.; Sobhani, H.; Lassiter, J. B.; Dorpe, P. V.; Nordlander, P.; Halas, N. J. Plasmonic Nanoclusters: Near Field Properties of the Fano Resonance Interrogated with SERS. *Nano Lett.* **2012**, *12*, 1660−1667.
(24) Maye, M. M.; Kumara, M. T.; Nykypanchuk, D.; Sherman, W. B.; Gang, O. Switching Binary States of Nanoparticle Superlattices and Dimer Clusters by DNA Strands. *Nat. Nanotechnol.* **2010**, *5*, 116−120.
(25) Mastroianni, A. J.; Claridge, S. A.; Alivisatos, A. P. Pyramidal and Chiral Groupings of Gold Nanocrystals Assembled Using DNA Scaffolds. *J. Am. Chem. Soc.* **2009**, *131*, 8455−8459.
(26) Tan, S. J.; Campolongo, M. J.; Luo, D.; Cheng, W. Building Plasmonic Nanostructures with DNA. *Nat. Nanotechnol.* **2011**, *6*, 268−276.
(27) Hong, S.; Kang, T.; Choi, D.; Choi, Y.; Lee, L. P. Self-Assembled Three-Dimensional Nanocrown Array. *ACS Nano* **2012**, *6*, 5803−5808.
(28) Maier, S. A. *Plasmonics: Fundamentals and Applications*; Springer: Berlin, 2007.

(29) Wustholz, K. L.; Henry, A.-I.; McMahon, J. M.; Freeman, R. G.; Valley, N.; Piotti, M. E.; Natan, M. J.; Schatz, G. C.; Van Duyne, R. P. Structure-Activity Relationships in Gold Nanoparticle Dimers and Trimers for Surface-Enhanced Raman Spectroscopy. *J. Am. Chem. Soc.* **2010**, *132*, 10903−10910.
(30) Choi, D.; Lee, S.; Kim, S.; Lee, P.; Lee, K.; Park, H.; Hwang, W. Dependence of Adhesion and Friction on Porosity in Porous Anodic Alumina Films. *Scr. Mater.* **2008**, *58*, 870−873.
(31) Choi, D.; Kim, S.; Lee, S.; Kim, D.; Lee, K.; Park, H.; Hwang, W. Structure-dependent Adhesion and Friction on Highly Ordered Metallic Nanopore Membranes. *Nanotechnology* **2008**, *19*, 145708.
(32) Giermann, A. L.; Thompson, C. V. Solid-state Dewetting for Ordered Arrays of Crystallographically Oriented Metal Particles. *Appl. Phys. Lett.* **2005**, *86*, 121903.
(33) Yang, S.; Xu, F.; Ostendorp, S.; Wilde, G.; Zhao, H.; Lei, Y. Template-confined Dewetting Process to Surface Nanopatterns: Fabrication, Structural Tunability, and Structure-related Properties. *Adv. Funct. Mater.* **2011**, *21*, 2446−2455.
(34) Lu, Y.; Xiong, H.; Jiang, X.; Xia, Y. Asymmetric Dimers can be Formed by Dewetting Half-Shells of Gold Deposited on the Surfaces of Spherical Oxide Colloids. *J. Am. Chem. Soc.* **2003**, *125*, 12724−12725.
(35) Knight, M.; Wu, W. Y.; Lassiter, J. B.; Nordlander, P.; Halas, N. J. Substrates Matter: Influence of an Adjacent Dielectric on an Individual Plasmonic Nanoparticle. *Nano Lett.* **2009**, *9*, 2188−2192.
(36) Gehr, R. J.; Boyd, R. W. Optical Properties of Nanostructured Optical Materials. *Chem. Mater.* **1996**, *8*, 1807−1819.
(37) Brandl, D. W.; Mirin, N. A.; Nordlander, P. Plasmon Modes of Nanosphere Trimers and Quadrumers. *J. Phys. Chem. B* **2006**, *110*, 12302−12310.
(38) Chuntonov, L.; Haran, G. Effect of Symmetry Breaking on the Mode Structure of Trimeric Plasmonic Molecules. *J. Phys. Chem. C* **2011**, *115*, 19488−19495.
(39) Sohn, A.; Gwon, M.; Choi, D.; Kim, D.-W. Plasmonic Coupling in Three-Dimensional Au Nanoparticle Assemblies Fabricated by Anodic Aluminum Oxide Templates. *J. Nanomater.* **2013**, *2013*, 823729.
(40) Choi, D.; Shin, C. K.; Yoon, D.; Chung, D. S.; Jin, Y. W.; Lee, L. P. Plasminc Optical Interference. *Nano Lett.* **2014**, *14*, 3374−3381.
(41) Hildebrandt, P.; Stockburger, M. Surface-enhanced Resonance Raman Spectroscopy of Rhodamine 6G Adsorbed on Colloidal Silver. *J. Phys. Chem.* **1984**, *88*, 5935−5944.